

# PubMed-Ophtha: An open resource for training ophthalmology vision-language models on scientific literature

Verena Jasmin Hallitschke<sup>\*a,b</sup>, Carsten Eickhoff<sup>c</sup> and Philipp Berens<sup>a,b</sup>

<sup>a</sup>Hertie Institute for AI in Brain Health, University of Tübingen, Tübingen, Germany

<sup>b</sup>Tübingen AI Center, Tübingen, Germany

<sup>c</sup>Institute for Applied Medical Informatics, University of Tübingen, Tübingen, Germany

This manuscript was compiled on May 5, 2026

**Abstract**—Vision-language models hold considerable promise for ophthalmology, but their development depends on large-scale, high-quality image-text datasets that remain scarce. We present PubMed-Ophtha, a hierarchical dataset of 102,023 ophthalmological image-caption pairs extracted from 15,842 open-access articles in PubMed Central. Unlike existing datasets, figures are extracted directly from article PDFs at full resolution and decomposed into their constituent panels, panel identifiers, and individual images. Each image is annotated with its imaging modality – color fundus photography, optical coherence tomography, retinal imaging, or other – and a mark status indicating the presence of annotation marks such as arrows. Figure captions are split into panel-level subcaptions using a two-step LLM approach, achieving a mean average sentence BLEU score of 0.913 on human-annotated data. Panel and image detection models reach a mAP@0.50 of 0.909 and 0.892, respectively, and figure extraction achieves a median IoU of 0.997. To support reproducibility, we additionally release the human-annotated ground-truth data, all trained models, and the full dataset generation pipeline.

**Keywords**—fundus image, optical coherence tomography, vision-language model, multimodal data, medical AI

## 1. BACKGROUND & SUMMARY

The ability to jointly reason over images and text has made vision-language models (VLMs) increasingly attractive for medicine, where they promise to automate tasks such as medical report generation and clinical question-answering [20]. Their development, however, depends on large corpora of high-quality image-text pairs – a resource that remains scarce in most clinical specialties. In ophthalmology, previous works have created datasets with retinal images such as color fundus photography (CFP) and optical coherence tomography (OCT) using a variety of textual sources. Datasets pairing retinal images with expert-written reports, such as DeepEyeNet [16], are few and small: annotation requires clinical expertise, data privacy constraints limit scale, and the reports themselves can be inconsistent owing to the time pressure under which they are produced [2, 6]. To increase scale, other approaches have paired images from existing classification benchmarks with automatically generated captions, either using fixed text templates or by substituting medical synonyms from a dictionary [23, 27]. For both approaches, however, caption diversity remains limited.

More recently, large-scale datasets have been assembled automatically from peer-reviewed biomedical literature available in open-access repositories [11, 22, 24, 26, 29, 31]. These datasets, however, share several limitations: many are not publicly available [29, 31], most are not specific to ophthalmology [11, 22, 24, 26, 29], and all rely on the pre-extracted figure images provided in PubMed Central article packages, which are compressed and therefore of lower resolution than the original images. Beyond image quality, none of these datasets account for the hierarchical structure of article figures — which are typically composed of labeled panels, each potentially containing multiple images — nor do they record the presence of annotation marks such as arrows or bounding boxes, which direct the reader’s attention to clinically relevant regions and could serve as valuable supervisory signal when training a VLM.

We present PubMed-Ophtha, a large-scale, hierarchical dataset of ophthalmological image-caption pairs that directly addresses these limitations. It contains 102,023 image-caption pairs extracted from

15,842 open-access articles. Unlike existing datasets, figures are extracted directly from article PDFs at full resolution and decomposed into their hierarchical structure of panels, panel identifiers, and individual images. Each image is annotated with its ophthalmological imaging modality and the presence of marks such as arrows, and captions are split into panel-level subcaptions, increasing semantic correspondence between images and text. To support reproducibility and further development, we additionally release the human-annotated ground-truth data (PubMed-Ophtha-Annotation) used for evaluating the models, all trained models, and the full dataset generation pipeline.

## 2. METHODS

### 2.1. Overview

The PubMed-Ophtha dataset was constructed through a four-stage pipeline (Figure 1). First, PubMed Central was filtered to identify articles relevant to retinal imaging, using a combination of figure captions, article key terms, and Medical Subject Headings (Figure 1A, B). Second, figures and their captions were extracted directly from the article PDFs at full resolution using a heuristic-based approach, and matched to their corresponding entries in the BIOMEDICA [26] dataset to retrieve additional figure-level information such as in-text mentions (Figure 1 C). Third, each figure was decomposed into its constituent panels, panel identifiers, and images using a set of detection models; each image was further assigned an image type and a mark status (Figure 1D). Fourth, figure captions were split into panel-level subcaptions and assigned to their corresponding panels, combining OCR-based matching, LLM-based refinement, and manual resolution where necessary. The result is a hierarchically structured dataset in which each panel is associated with an image, an image type, a mark status, and a subcaption.

**Table 1.** Overview of the models used in the dataset processing pipeline.

Step	Model	Data
Panel Detection	RetinaNet	PubMed-Ophtha-Annotation
Image Detection	RetinaNet	PubMed-Ophtha-Annotation
Mark Status Classification	ResNet-50	PubMed-Ophtha-Annotation
Caption Splitting	Qwen3 32B-AWQ	PubMed-Ophtha-Annotation
Optical Character Recognition	EasyOCR (CRNN [10])	–
Panel Assembly	Qwen3-VL 30B-A3B	Manual

### 2.2. Terminology

We use the following terminology throughout (Figure 1 C, D). A figure refers to the complete visual element as it appears in the publication, potentially comprising multiple components. Each such component is called a panel and is typically distinguished by a panel identifier — a letter (A, B, C), number, or positional descriptor (top, left, right) appearing in the caption, on the figure, or both. Figures without any panel identifiers are treated as single-panel figures. A panel may

\*verena-jasmin.hallitschke@uni-tuebingen.de (V. Hallitschke)

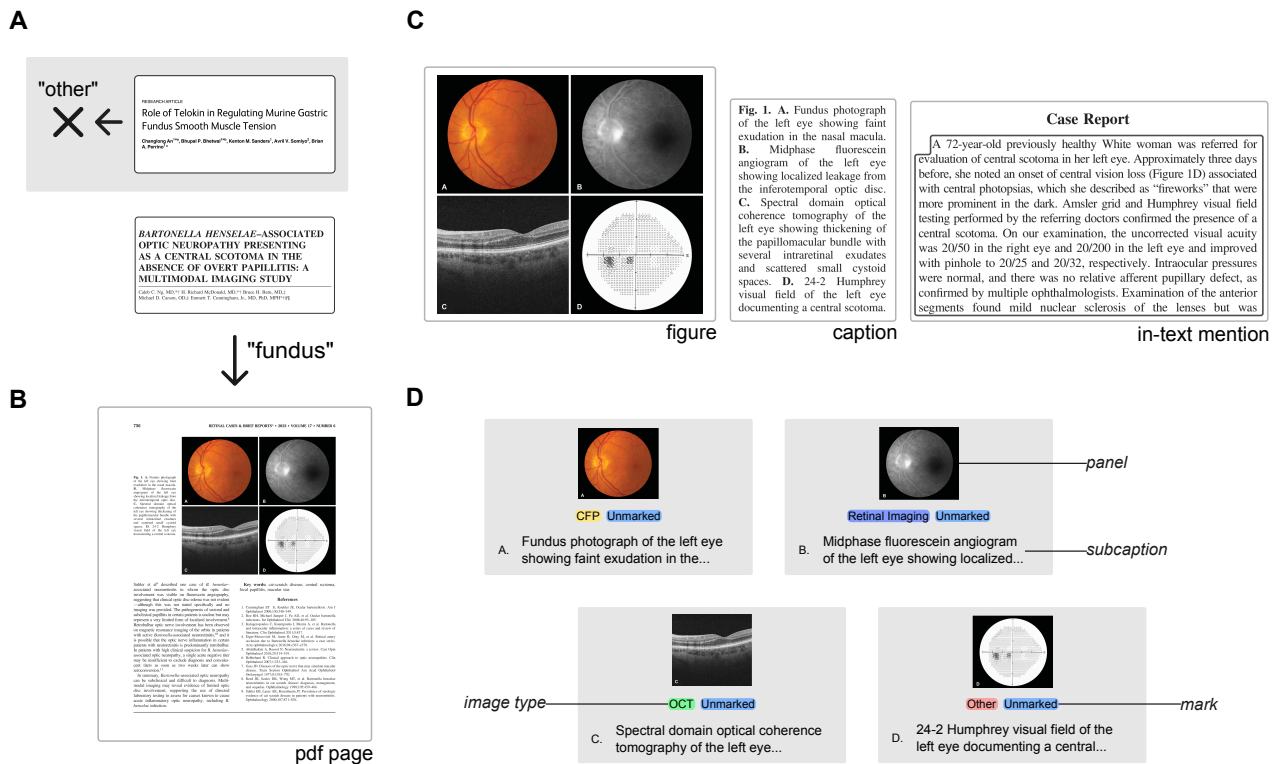


**Figure 1.** Overview of the dataset extraction pipeline. (A) Articles are filtered by keywords to select those relevant to ophthalmological retinal imaging. (B) A heuristic detects figures and their captions in the article PDF and extracts them at full resolution. (C) Additional figure-level information, such as in-text mentions, is retrieved from the BIOMEDICA dataset. (D) The final dataset contains individual panels with their subcaptions, image type annotations, and mark status.

contain one or more images, defined here as bitmap representations of an ophthalmic acquisition such as a CFP or OCT scan, as well as other elements such as graphs or text. The caption refers to the full figure caption as published; a subcaption is the portion of the caption corresponding to a single panel. An in-text mention is any reference to a figure appearing in the article body. Each image is assigned an image type (CFP, OCT, Retinal Imaging, or Other) and a mark status, indicating whether the image contains annotations — such as arrows or bounding boxes — that highlight a region of interest.

### 2.3. Filtering PubMed Central for Ophthalmological Articles

PubMed Central (PMC) is one of the largest openly available corpora of biomedical literature, containing over 10 million<sup>1</sup> articles across a broad range of domains. In PMC, articles are provided either as a standalone PDF or as a package comprising the PDF, a machine-readable XML file, and the article figures as JPEG images; the latter were often compressed and therefore of lower resolution than the figures in the original PDF. Article metadata was fully searchable via the NCBI Entrez Programming Utilities [4]. The BIOMEDICA dataset [26] built on PMC by providing its figure-caption corpus as an easily processable webdataset, enriched with automatically detected figure-type labels. We constructed our dataset by combining data from BIOMEDICA, which provided convenient access to figure captions and figure-type labels, with data extracted directly from the article PDFs available through the PMC FTP services, as well as article metadata retrieved via Entrez.

We selected articles relevant to retinal imaging by filtering on keywords drawn from figure captions, article key terms, and Medical Subject Headings (MeSH). The imaging keywords used were "color fundus photography", "CFP", "optical coherence tomography", and "OCT" (Figure 1 A). An article was retained if it satisfied at least one criterion from each of the following three levels: (i) at least one figure or table caption contained an imaging keyword or the word "fundus";

<sup>1</sup><https://pmc.ncbi.nlm.nih.gov/about/intro/>

(ii) the article key terms included an imaging keyword or the word "retina", or the MeSH terms included "optical coherence tomography" or "ophthalmoscopy"; and (iii) the full text contained "retina" or "ophthalmology", or the MeSH terms included "fundus oculi" or "retina". Additionally, articles in the BIOMEDICA dataset containing at least one figure labeled as OCT were retained if they met criterion (ii). After this filtering step, 24,781 articles remained from the 5 million articles with figures in the BIOMEDICA dataset.

### 2.4. Extracting High-Resolution Figures from Article PDFs

To ensure high-resolution figures, we extracted figures and their captions directly from the article PDFs (Figure 1B), rather than relying on the compressed JPEG images provided in the PMC article packages. Each page was processed separately through four steps. First, candidate figures were detected by analyzing the internal PDF layout and merging proximate bitmap and vector graphics; elements that were too small or located in the page margin were discarded as likely page header artifacts. Second, each text segment on the page was assigned a caption likelihood score for each candidate figure. This score increased if the text began with or contained the word "figure", if the text was spatially close to and horizontally aligned with the figure's bounding box, and if it appeared below the figure; it decreased if other page elements intervened between the text and the figure, or if the text was positioned diagonally relative to it. Third, figures and captions were assigned to one another based on this score and their mutual distance, with conflicts — such as multiple captions per figure or multiple figures per caption — resolved heuristically. Fourth, the resulting text and figure bounding boxes were refined and merged with surrounding elements where appropriate. The figure identifier was extracted from the assigned caption using a regular expression.

Since the XML article files did not contain information about figure placement within the PDF, each extracted figure was matched to its corresponding entry in the BIOMEDICA dataset, enabling the figures to be linked back to the XML file and enriched with additional

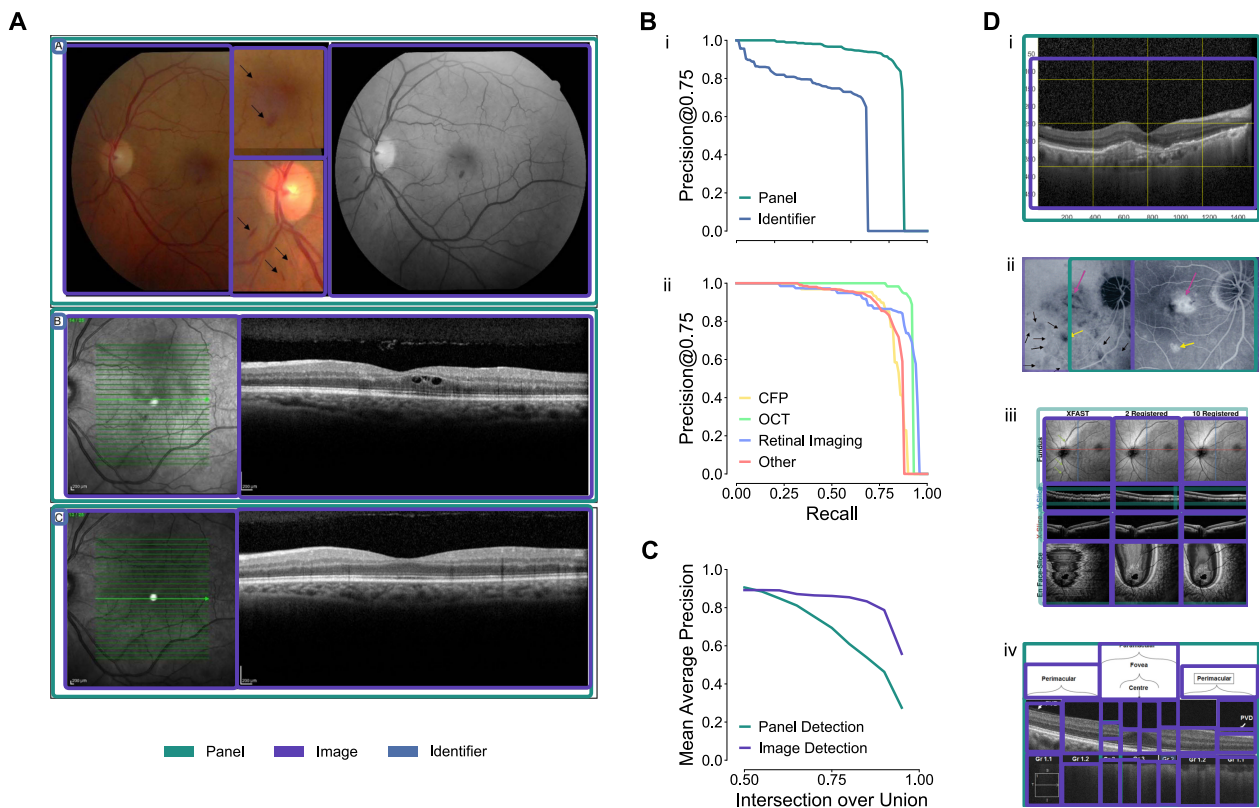


**Figure 2.** Detection performance and failure cases. (A) Example detections from the test set, showing panel (teal), image (purple), and panel identifier (blue) bounding boxes across three figures of varying complexity. (B) Precision-recall curves at an IoU threshold of 0.75 for (i) panel and panel identifier detection and (ii) image type detection across the four image type categories (CFP, OCT, Retinal Imaging, Other). (C) Mean average precision as a function of IoU threshold for the panel detection and image detection models. (D) Representative failure cases: (i) bounding boxes cropping the empty area at the top of OCT scans; (ii) incorrect panel division in figures lacking panel identifiers; (iii) clipping of embedded textual descriptions at panel boundaries; (iv) fragmentation of images due to confusion of visual guides with spatial separators.

features such as in-text mentions. Matching was based on similarity between the extracted figure and the corresponding image in the PMC package, assessed across four criteria: (i) the Hamming distance between perceptual image hashes did not exceed a threshold; (ii) the figure identifier extracted from the caption matched an identifier estimated from the package filename; (iii) the difference in aspect ratio was below a threshold; and (iv) the Levenshtein distance between the extracted caption and the caption in the BIOMEDICA dataset did not exceed a threshold. An extracted figure was assigned to a package entry if it passed at least two of these checks; where multiple extracted figures were matched to the same entry, only the one with the greatest number of similarity matches was retained. Figures spread across multiple pages in the PDF were joined during this step. In total, 74,121 figures were extracted from the 18,395 articles. The extraction process did not extract any figures from the remaining 6,386 articles.

## 2.5. Panel and Image Detection

### 2.5.1. Annotation Dataset

Having filtered articles and extracted their figures, the next step was to detect panels and images within each figure, along with their imaging type and mark status, using a set of trained detection and classification models. Existing datasets for figure parsing address only subsets of the annotations required here. The ImageCLEF2016 dataset [7] provides bounding box annotations for individual images within figures, while the PanelSeg dataset [15] annotates panels and panel identifiers. Neither dataset combines all three annotation types, and neither includes image type or mark status labels. The BIOMEDICA dataset provides image type annotations at the panel level, but does not cover the fundus imaging modalities relevant to our setting.

We therefore collected and manually annotated a dataset of 1,901

figures using Label Studio [14] in multiple annotation rounds (Supplementary Figures S1 - S3). In the first round, annotators were presented with each figure, its caption, and associated metadata, and were asked to correct proposed panel bounding boxes and assign image type and mark status labels at the panel level. The boxes were proposed by a model trained on the ImageCLEF2016 dataset. Where panel identifiers were positional (e.g., "first row"), annotators used the caption to determine panel positions. In figures with nested panel hierarchies, only the highest hierarchical level was annotated. Each panel was assigned one or more image types — OCT for OCT scans, CFP for narrow-angle color fundus photography, Retinal Imaging for ultra-wide field imaging and other retinal depictions such as fluorescein angiography, and Other for all remaining content such as graphs or ultrasound images — and a mark status indicating whether at least one image in the panel contained a mark, defined as an arrow, dot, or similar annotation referenced in the caption or labeled directly on the figure.

In the second round, annotators refined the panel annotations and added panel identifier bounding boxes. In the final round, individual image bounding boxes were added, each assigned exactly one image type and one mark status, with further refinement of existing bounding boxes where necessary. To support evaluation of the caption splitting step, the captions of 158 randomly selected figures were additionally annotated with subcaptions, textual panel identifiers, and associated panel bounding boxes.

The final annotated dataset contains panel, panel identifier, and image bounding boxes for 1,534 figures (Figure 2A). Of these, 158 also include per-panel subcaptions and panel identifier labels, and a further 351 contain only panel and panel identifier annotations, as the model already achieved sufficient performance on these samples. The remaining 16 figures were excluded: these comprised figures

whose panels could not be separated by bounding boxes, and figures whose subcaptions referenced marks rather than panels. This dataset, including bounding boxes and all other annotations is available as PubMed-Ophtha-Annotation.

### 2.5.2. Detection Pipeline

Separating figures into their constituent panels and images is a multi-task problem, comprising panel detection, panel identifier detection, and image detection. Because each image is assigned both an image type and a mark status, image detection is in turn a multi-label task. To avoid the complexity of a joint multi-label detection setting – which would prevent the use of task-specific pretraining weights and architectures, and risk conflating panel-level and image-level predictions – we decomposed the problem into three separate models: two multi-class bounding box detectors and one binary mark status classifier. Running two detection models independently also introduced a natural fallback, where the output of one could be used to refine the other during assignment.

For both bounding box detection tasks, we used a Detectron2 [13] to fully finetune a RetinaNet [9] with a ResNet-50 [8] backbone, pre-trained on MS-COCO [5] and subsequently finetuned on the ImageCLEF2016 dataset [7]. For each task, six models were trained with different random seeds and the best model was selected based on validation mAP at an IoU threshold of 0.90.

The first model detected panels and panel identifiers. We merged our annotated dataset with the PanelSeg dataset [15], resampling PanelSeg to remove overlap with the ImageCLEF2016 training, validation, and test splits. The merged dataset was used to finetune the ImageCLEF2016-pretrained model for 100,000 iterations with a batch size of 16 on 1 NVIDIA A100 GPU. The best model reached an mAP@0.90 of 0.463 after 26,865 iterations (mAP@0.50: 0.906). The second model detected images and assigned their image types. It was finetuned from the same ImageCLEF2016-pretrained checkpoint on our collected image type annotations for 15,000 iterations with a batch size of 16 on 1 NVIDIA V100 GPU, reaching an mAP@0.90 of 0.787 after 3,909 iterations (mAP@0.50: 0.892).

The mark status classifier was a ResNet-50 with ImageNet [3] initialization, trained on our annotated dataset for 35 epochs with a batch size of 32. Six models were trained with different random seeds and the best was selected based on validation accuracy, reaching 89.5% after 7 epochs. During training, the input image was augmented with random cropping, flips, affine transformations, and color augmentations to make the model robust to errors in the figure extraction and image detection. The cropping augmentation operated on the full figure and randomly perturbed each corner of the ground truth bounding box asymmetrically, shifting it outward by up to 20% or inward by up to 30% of the box dimensions.

During inference, the panel detection and image detection models processed each figure independently. Detected bounding boxes were filtered using a score threshold of 0.25, followed by non-maximum suppression with an IoU threshold of 0.3; for the panel detection model, suppression was applied class-wise so that only boxes of the same type were compared. Figures were then cropped to the detected image bounding boxes, and the mark status classifier was applied to each cropped image individually.

Across 72,802 figures excluding the annotated dataset, this step yielded 262,104 panels, 448,090 images, and 226,562 panel identifiers. 18 figures were rejected due to missing detections.

## 2.6. Caption Splitting

Figure captions in medical publications are highly informative, often containing detailed descriptions of pathologies alongside references to specific panels. After detecting panels within a figure, captions were split into panel-level subcaptions to preserve this semantic correspondence (Figure 3A, B). The output of this step was a mapping

from each panel identifier to its corresponding subcaption.

Given the considerable variability in caption formatting across publications, we adopted an LLM-based approach. Initial experiments revealed that when prompted to split captions directly, the model struggled to reliably identify panel identifiers, often describing subcaption content instead. To address this, we decomposed the task into two sequential steps: the model first extracted all panel identifiers from the full caption, and then assigned the corresponding subcaption to each identifier. Captions for which no panel identifiers were found were treated as single-panel figures and assigned in full.

We used Qwen3 32B [28] using vLLM [19] with Action-aware Weight Quantization [21] and parsed all model outputs with Pydantic [30], a library for data validation that allows parsing of typed and structured JSON text. Separate system prompts were used for each of the two steps<sup>2</sup>. The model was provided with 17 manually annotated in-context examples for the panel identifier extraction step and 7 examples for the subcaption extraction step. In total, 72,756 captions excluding the annotated dataset were split into 245,693 subcaptions, 64 captions were discarded due to parsing errors.

## 2.7. Panel Assembly

After the previous processing steps, each figure was associated with a set of detected panels, a set of subcaptions with their panel identifiers, a set of panel identifier bounding box locations, and a set of detected images. The goal of this step was to merge these into a unified per-panel record, where each panel is associated with a subcaption and, where applicable, one or more images and panel identifier locations. Caption assignment was performed only for figures in which at least one image had an image type other than Other, leading to the rejection of 37,915 articles.

Assignment began with a geometric matching step. Images and panel identifier locations were assigned to panels based on IoU and overlap fraction, using thresholds of 0.3 and 0.7, respectively. For figures with alphabetic panel identifiers, subcaptions were assigned automatically by reading the panel identifier text at the detected panel identifier location using EasyOCR<sup>3</sup>; where no panel identifier was detected within a panel, OCR was applied to the full panel as a fallback.

Panels with missing or incomplete subcaption assignments were subsequently refined using an LLM-based approach. We deployed the thinking version of Qwen3-VL 30B-A3B [25] with vLLM and prompted the model independently twice per figure to increase assignment reliability. The model inputs, prompts, and output schemas varied depending on whether the panel identifiers in the caption were positional (e.g., *top*, *left*), allowing for more targeted processing in those cases<sup>4</sup>. When the two model responses conflicted, an adjudication step was performed in which both responses were provided to the model alongside a resolution prompt. All outputs were parsed with Pydantic, and the assignment was validated and re-prompted up to five times to ensure consistency.

In total, 98,639 panels were fully assigned, of which 67,175 were resolved automatically, 31,291 were refined by the LLM, and 173 required manual resolution.

Figures from PubMed-Ophtha-Annotation were additionally incorporated into the dataset, with ground-truth bounding boxes used in place of model predictions where available. For these figures, the automatic detection pipeline was applied only where annotations were absent, and panels were subsequently filtered to retain only those containing at least one retinal image. Captions were then split and panel assembly was performed following the same procedure as for the remainder of the dataset. Of the resulting panels, 584 originated

<sup>2</sup>[https://github.com/berenslab/pubmed-ophtha/blob/main/src/pubmed\\_ophtha/caption\\_splitting/messages.py](https://github.com/berenslab/pubmed-ophtha/blob/main/src/pubmed_ophtha/caption_splitting/messages.py)

<sup>3</sup><https://github.com/JaidedAI/EasyOCR>

<sup>4</sup>[https://github.com/berenslab/pubmed-ophtha/blob/main/src/pubmed\\_ophtha/panel\\_assembly/messages.py](https://github.com/berenslab/pubmed-ophtha/blob/main/src/pubmed_ophtha/panel_assembly/messages.py)

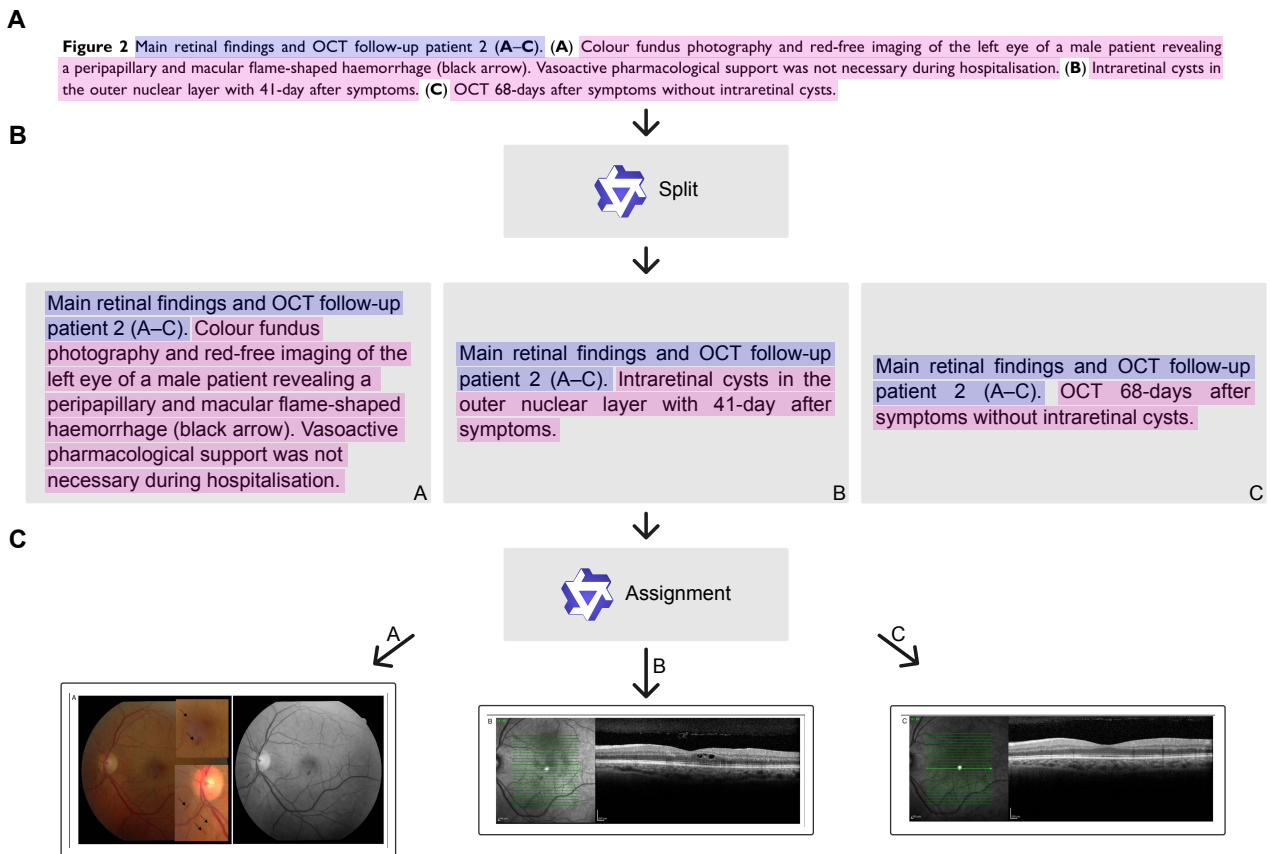


**Figure 3.** Caption splitting and subcaption assignment. (A) Original figure with its full caption. (B) Result of the caption splitting step: the full caption is decomposed into panel-level subcaptions, each associated with a panel identifier. (C) Result of the panel assembly step: each subcaption is assigned to its corresponding panel, and panel identifier locations are matched to the detected panel bounding boxes.

directly from fully annotated figures; the remaining panels were assembled using a combination of ground-truth bounding boxes and automatic processing, with 1,473 assigned automatically, 1,129 refined using the LLM, and 198 resolved manually. The final dataset consists of 102,023 panels from 35,544 figures across 15,842 articles.

### 3. DATA RECORDS

The PubMed-Ophtha dataset and the collected training datasets are available on Hugging Face Datasets<sup>5</sup> [18] and are split into one Parquet and one JSON file. The PubMed-Ophtha dataset is provided in a panel-centric format in the `pubmed_ophtha.parquet` file to facilitate the training of VLMs. In the file, each row represents a panel from a figure with a unique `panel_id` and a set of features, including the panel as binary image, the subcaption text and binary imaging type and mark status indicators. The full list of columns in the file and their descriptions can be found in Table 2. The `position` column contains a JSON-serialized dictionary with four entries: `predicted_box`, the panel bounding box as predicted by the panel detection model; `content_box`, the final bounding box encompassing all panel contents including associated images and panel identifiers; both normalized to figure dimensions (left, top, right, bottom in the range [0, 1]); `figure_page_coordinates`, the figure position in PDF page coordinates; and `prediction_score`, the detection confidence of the predicted panel bounding box. The `image_data` and `identifier_data` columns contain JSON-serialized lists of the images and panel identifiers associated with the panel. Each entry stores its bounding box in the `position` field as a JSON-serialized dictionary containing `predicted_box` – coordinates normalized relative to the figure dimensions (left, top, right, bottom in the range [0, 1]), and a `prediction_score`. Each image additionally has an `imaging_type` field with a label and prediction score, a

`mark_status` field indicating whether the image contains annotation marks, and flags indicating whether it originates from ground-truth annotation (`is_gt`) and whether it is used to calculate the panel content box (`included_in_content_box`). Each panel identifier entry similarly contains `is_gt`, `included_in_content_box`, and an `origin_identifier` field linking back to the detection from which it was derived. Note that neither the PMC ID nor the image cluster ID alone uniquely identifies a figure, as only their combination does. Fig. 4 shows several examples from the dataset.

The second file, `pubmed_ophtha_annotation.json`, is the PubMed-Ophtha-Annotation dataset, where each entry corresponds to one figure. Each figure is uniquely identified by the combination of its `article_id` and `image_cluster_id` and has a list of figure and caption locations and a list of panels. The locations of the figures and captions are provided as a list because the figures can spread across multiple pages, while the positions of the panels, images, and labels are normalized in figure space. Table 3 contains an overview of the fields in the JSON file.

For some figures, features such as the panel images and subcaptions are not available upon download due to license restrictions. These fields can be populated using the scripts in the repository. Additionally, the repository contains examples for data loading and usage in Python<sup>6</sup>.

### 4. DATA OVERVIEW

The final dataset contains 102,023 panels from 35,544 figures across 15,842 open-access articles. Key statistics on image type distribution, mark status, subcaption length, and panel assembly method are summarized in Table 4.

<sup>5</sup><https://huggingface.co/datasets/pubmed-ophtha/PubMed-Ophtha>

<sup>6</sup><https://github.com/berenslab/pubmed-ophtha/tree/main/examples>

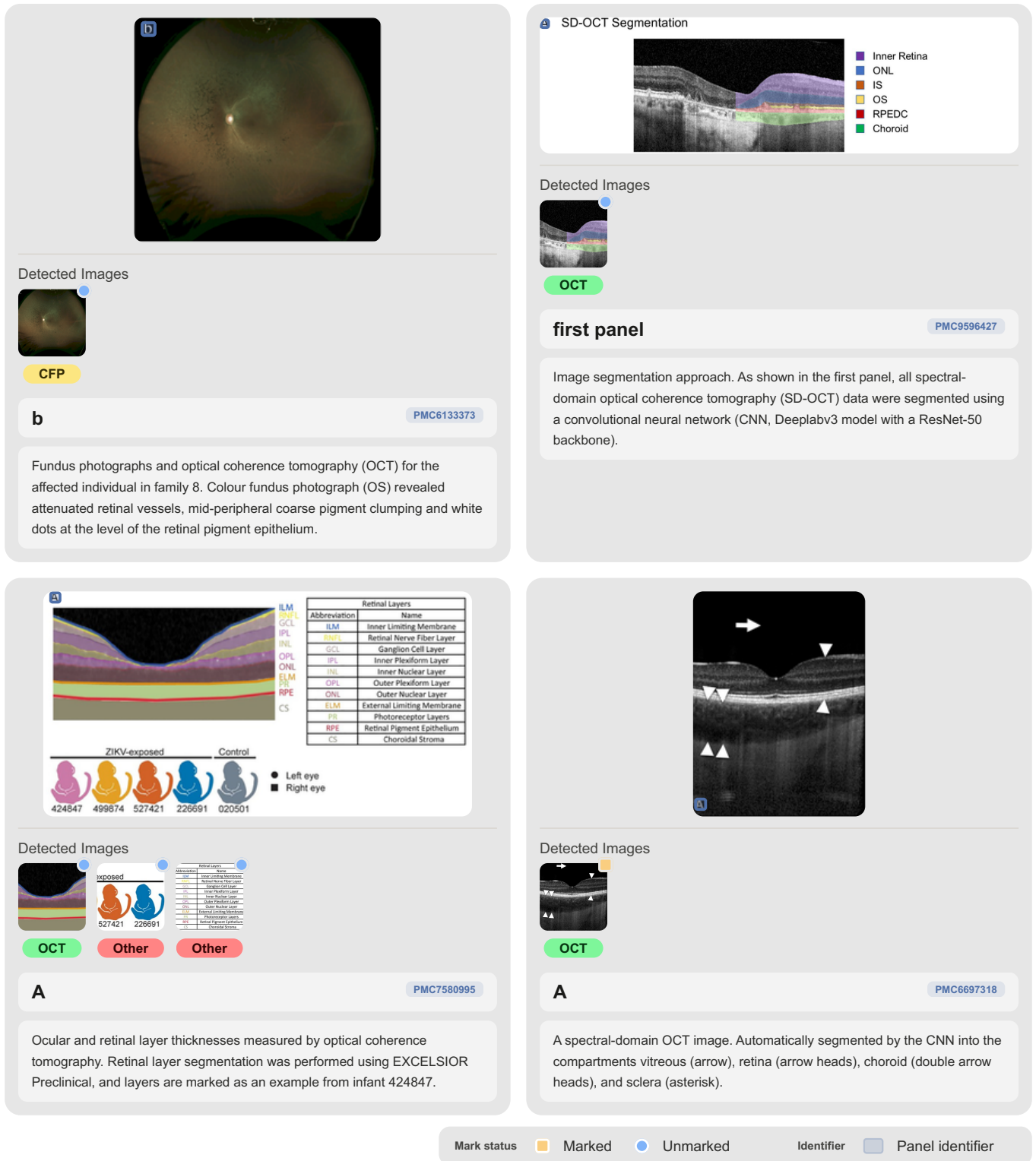


Figure 4. Examples of extracted panels with their identifiers, subcaptions, and the detected images.

## 5. TECHNICAL VALIDATION

We validated every step of the dataset extraction pipeline carefully (Figure 1) treating the performance of each trained model on held-out human-annotated data as a proxy for the quality of the resulting image-caption pairs. Validation covered figure extraction, panel and image detection, imaging type and mark status classification, caption splitting, and caption assignment.

### 5.1. Validation of the Detection Pipeline

Both detection models performed well overall, reliably localizing panels, images, and panel identifiers across a range of figure layouts (Figure 2A). We evaluated performance on a held-out test set of 188 figures (panel detection), 157 figures (image detection), and 1,054 images (mark status classification) using precision-recall curves at an IoU threshold of 0.75 and mean average precision (mAP) as a function of IoU (Figure 2B, C).

Panel detection was robust, with mAP degrading from 0.909 at IoU 0.50 to 0.532 at IoU 0.95, and precision remaining high across most of the recall range (Figure 2Bi, C). Panel identifier detection was considerably weaker, with mAP dropping from 0.903 at IoU 0.50 to 0.018 at IoU 0.95 and precision deteriorating sharply beyond a recall of 0.6 (Figure 2Bi). This disparity indicates that panel identifier detection is the primary source of overall performance degradation. However, errors at this stage can be partially compensated during panel assembly, where image bounding boxes and LLM-based refinement provide an additional fallback.

Image detection generalized well across IoU thresholds, with mAP declining from 0.892 at IoU 0.50 to 0.558 at IoU 0.95 (Figure 2C). Precision-recall curves were stable across the CFP, OCT, and Retinal Imaging categories, while the Other category showed lower performance across all IoU values (mAP@0.50: 0.855, mAP@0.95: 0.324), likely reflecting the greater visual heterogeneity of this class (Figure 2Bii). The mark status classification model reached an accuracy of 89.5% on the test set.

The models handled the majority of figure layouts well, and failure cases follow recognizable patterns that can be partially addressed downstream (Figure 2D). In OCT images, bounding boxes occasionally crop the empty area at the top of the scan, though the diagnostically relevant content is mostly retained (Figure 2Di). In figures lacking panel identifiers, panels are sometimes fragmented or incorrectly divided, but these cases are amenable to correction through LLM-based refinement during panel assembly (Figure 2Dii). Textual descriptions embedded within panels are occasionally clipped at panel boundaries, which can affect subcaption assignment for the corresponding images (Figure 2Diii). Finally, in figures with complex layouts, annotation marks or visual guides may be detected as separate Other-type images or cause image bounding boxes to fragment across spatial separators; such spurious detections can be identified and filtered in post-processing (Figure 2Div).

The performance of the figure extraction process was ensured by manual evaluation of 100 randomly sampled article PDF files. Additionally, we manually annotated the ground truth locations of the figures in the collected dataset and measured a median IoU of 0.997.

## 5.2. Validation of the Caption Splitting Approach

Caption splitting involves two sequential tasks (Figure 3): extracting panel identifiers from the full caption, and assigning the corresponding subcaption to each identifier. We evaluated both tasks on the human-annotated subset of the dataset. During evaluation, predicted subcaptions were matched to ground truth values by normalizing and aligning panel identifiers; only samples where all panel identifiers could be matched were used to assess subcaption quality. The proportion of unprocessed samples, therefore, serves as a proxy for panel identifier extraction performance.

The two-step decomposition substantially improved panel identifier extraction. In the three-shot setting, extracting panel identifiers as a separate first step reduced the proportion of unprocessed samples from 18.4% to 10.6%. Increasing the number of few-shot examples for the identifier extraction step from three to thirteen reduced this further to 7.8%. The remaining errors fell into three categories: missing panel identifiers, extraction of additional hierarchical levels, and identifier mismatches requiring more complex normalization. The latter two can be resolved during panel assembly, and samples affected by the first can often be at least partially processed.

Subcaption quality was measured using the mean average sentence BLEU score (maB), computed per sample using SacreBLEU [12] and the sentence BLEU metric [1]. Performance improved markedly with the addition of few-shot examples: enabling thinking mode in the zero-shot setting raised the maB from 0.634 to 0.682, and providing three examples increased it to 0.887. Introducing the two-step process had only a minimal effect on the maB itself (0.885 at 3-shot, 0.876 at 13-shot), likely because the gain in processable samples partially

offset the per-sample score. The final configuration — 17 few-shot examples for panel identifier extraction and 7 for subcaption assignment — achieved an maB of 0.913 with 6.4% of samples unprocessed, demonstrating that high subcaption quality and broad coverage can be achieved simultaneously. Common errors were the failure to remove the panel identifiers from the subcaption text, failure to add text that concerns all panels to the subcaptions, such as introductory phrases or lists of abbreviations, and slight rephrasing. As an example of this rephrasing, the model extracts the subcaption "SEM image of sample iPP/CuNPs 0.25 wt % at 5000× magnification." from "SEM images with different magnification (a) 5000, (b) 30,000, (c) 30,000, and (d) 100,000 times of sample iPP/CuNPs 0.25 wt %." [17]. The corresponding ground truth annotation "SEM images with magnification 5000 times of sample iPP/CuNPs 0.25 wt %." is semantically equivalent to the predicted subcaption. Overall, these errors have only a minor impact on dataset quality, as the resulting subcaptions remain semantically equivalent to the ground truth in the majority of cases.

## 5.3. Caption Assignment

The LLM refinement adds a fallback layer for errors in the extracted panel identifiers, as slight identifier mismatches and superfluous subcaptions can be resolved here. Prompting the model twice and an optional third adjudication step increase the stability of the assignment output. Furthermore, the functionality of the caption assignment was validated on a randomly sampled selection of 50 figures, out of which 25 were automatically assigned and 25 used LLM refinement. In total 88% of the panels were correctly assigned and 6% were incorrectly assigned. The remaining 6% of the entries had panel bounding boxes that spanned multiple panels and could therefore not be evaluated. In those cases the assigned panel was among the spanned panels. Notably, all of the automatically assigned panels in the test had the correct assignment.

## 6. DATA AVAILABILITY

The datasets are available on Hugging Face Datasets<sup>7</sup>. The `pubmed_ophtha.parquet` file contains the PubMed-Ophtha dataset in a panel-centric format, and `pubmed_ophtha_annotation.json` contains the ground-truth annotations from the PubMed-Ophtha-Annotation dataset.

## 7. CODE AVAILABILITY

The code used to create this dataset is available on GitHub<sup>89</sup> under the MIT license.

<sup>7</sup><https://huggingface.co/datasets/pubmed-ophtha/PubMed-Ophtha>

<sup>8</sup><https://github.com/berenslab/pubmed-ophtha>

<sup>9</sup><https://github.com/berenslab/pmo-parser>

## REFERENCES

- [1] K. Papineni, S. Roukos, T. Ward, and W.-J. Zhu, “Bleu: A Method for Automatic Evaluation of Machine Translation”, in *Proceedings of the 40th Annual Meeting of the Association for Computational Linguistics*, P. Isabelle, E. Charniak, and D. Lin, Eds., Philadelphia, Pennsylvania, USA: Association for Computational Linguistics, Jul. 2002, pp. 311–318.
- [2] B. I. Reiner, N. Knight, and E. L. Siegel, “Radiology reporting, past, present, and future: The radiologist’s perspective”, *Journal of the American College of Radiology*, vol. 4, no. 5, pp. 313–319, 2007, ISSN: 1546-1440.
- [3] J. Deng, W. Dong, R. Socher, L.-J. Li, K. Li, and L. Fei-Fei, “ImageNet: A large-scale hierarchical image database”, in *2009 IEEE Conference on Computer Vision and Pattern Recognition*, Jun. 2009, pp. 248–255.
- [4] *Entrez Programming Utilities Help*. National Center for Biotechnology Information (US), 2010.
- [5] T.-Y. Lin et al., “Microsoft COCO: Common Objects in Context”, in *Computer Vision – ECCV 2014*, D. Fleet, T. Pajdla, B. Schiele, and T. Tuytelaars, Eds., Cham: Springer International Publishing, 2014, pp. 740–755, ISBN: 978-3-319-10602-1.
- [6] N. Clynych and J. Kellett, “Medical documentation: Part of the solution, or part of the problem? A narrative review of the literature on the time spent on and value of medical documentation”, *International Journal of Medical Informatics*, vol. 84, no. 4, pp. 221–228, 2015, ISSN: 1386-5056.
- [7] A. G. S. De Herrera, S. Bromuri, R. Schaer, and H. Müller, “Overview of the medical tasks in ImageCLEF 2016”, *CLEF working notes*. Evora, Portugal, 2016.
- [8] K. He, X. Zhang, S. Ren, and J. Sun, “Deep Residual Learning for Image Recognition”, in *2016 IEEE Conference on Computer Vision and Pattern Recognition (CVPR)*, Las Vegas, NV, USA: IEEE, Jun. 2016, pp. 770–778, ISBN: 978-1-4673-8851-1.
- [9] T.-Y. Lin, P. Goyal, R. Girshick, K. He, and P. Dollár, “Focal Loss for Dense Object Detection”, in *Proceedings of the IEEE international conference on computer vision*, 2017, pp. 2980–2988.
- [10] B. Shi, X. Bai, and C. Yao, “An end-to-end trainable neural network for image-based sequence recognition and its application to scene text recognition”, *IEEE Trans. Pattern Anal. Mach. Intell.*, vol. 39, no. 11, pp. 2298–2304, Nov. 2017, ISSN: 0162-8828.
- [11] O. Pelka, S. Koitka, J. Rückert, F. Nensa, and C. M. Friedrich, “Radiology objects in context (roco): A multimodal image dataset”, in *Intravascular Imaging and Computer Assisted Stenting and Large-Scale Annotation of Biomedical Data and Expert Label Synthesis*, D. Stoyanov et al., Eds., Cham: Springer International Publishing, 2018, pp. 180–189, ISBN: 978-3-030-01364-6.
- [12] M. Post, “A call for clarity in reporting BLEU scores”, in *Proceedings of the Third Conference on Machine Translation: Research Papers*, Belgium, Brussels: Association for Computational Linguistics, Oct. 2018, pp. 186–191.
- [13] Y. Wu, A. Kirillov, F. Massa, W.-Y. Lo, and R. Girshick, *Detectron2*, 2019. [Online]. Available: <https://github.com/facebookresearch/detectron2>
- [14] M. Tkachenko, M. Malyuk, A. Holmanyuk, and N. Liubimov, *Label Studio: Data labeling software*, 2020. [Online]. Available: <https://github.com/HumanSignal/label-studio>
- [15] J. Zou, G. Thoma, and S. Antani, “Unified deep neural network for segmentation and labeling of multipanel biomedical figures”, *J. Assoc. Inf. Sci. Technol.*, vol. 71, no. 11, pp. 1327–1340, Oct. 21, 2020, ISSN: 2330-1635.
- [16] J.-H. Huang et al., “DeepOpht: Medical Report Generation for Retinal Images via Deep Models and Visual Explanation”, in *2021 IEEE Winter Conference on Applications of Computer Vision (WACV)*, Waikoloa, HI, USA: IEEE, Jan. 2021, pp. 2441–2451, ISBN: 978-1-6654-0477-8.
- [17] N. Jardón-Maximino et al., “Antimicrobial property of polypropylene composites and functionalized copper nanoparticles”, *Polymers*, vol. 13, no. 11, p. 1694, 2021.
- [18] Q. Lhoest et al., “Datasets: A Community Library for Natural Language Processing”, in *Proceedings of the 2021 Conference on Empirical Methods in Natural Language Processing: System Demonstrations*, Association for Computational Linguistics, Nov. 2021, pp. 175–184.
- [19] W. Kwon et al., “Efficient memory management for large language model serving with pagedattention”, in *Proceedings of the ACM SIGOPS 29th Symposium on Operating Systems Principles*, 2023.
- [20] I. Hartsock and G. Rasool, “Vision-language models for medical report generation and visual question answering: A review”, *Frontiers in artificial intelligence*, vol. 7, p. 1 430 984, 2024.
- [21] J. Lin et al., “Awq: Activation-aware weight quantization for llm compression and acceleration”, in *MLSys*, 2024.
- [22] J. Rückert et al., “Rocov2: Radiology objects in context version 2, an updated multimodal image dataset”, *Scientific Data*, vol. 11, no. 1, p. 688, 2024.
- [23] Q. Yu et al., “Clip-dr: Textual knowledge-guided diabetic retinopathy grading with ranking-aware prompting”, in *Medical Image Computing and Computer Assisted Intervention – MICCAI 2024: 27th International Conference, Marrakesh, Morocco, October 6–10, 2024, Proceedings, Part I*, Marrakesh, Morocco: Springer-Verlag, 2024, pp. 667–677, ISBN: 978-3-031-72377-3.
- [24] N. Baghbanzadeh et al., “Advancing Medical Representation Learning Through High-Quality Data”, pp. 24–33, 2025.
- [25] S. Bai et al. “Qwen3-VL Technical Report”. arXiv: 2511.21631 [cs], pre-published.
- [26] A. Lozano et al., “BIOMEDICA: An Open Biomedical Image-Caption Archive, Dataset, and Vision-Language Models Derived from Scientific Literature”, in *2025 IEEE/CVF Conference on Computer Vision and Pattern Recognition (CVPR)*, Jun. 2025, pp. 19 724–19 735.
- [27] J. Silva-Rodríguez, H. Chakor, R. Kobbi, J. Dolz, and I. Ben Ayed, “A foundation language-image model of the retina (flair): Encoding expert knowledge in text supervision”, *Medical Image Analysis*, vol. 99, p. 103 357, 2025, ISSN: 1361-8415.
- [28] A. Yang et al. “Qwen3 Technical Report”. arXiv: 2505.09388 [cs], pre-published.
- [29] S. Zhang et al., “A Multimodal Biomedical Foundation Model Trained from Fifteen Million Image–Text Pairs”, *NEJM AI*, vol. 2, no. 1, Jan. 2025, ISSN: 2836-9386.
- [30] S. Colvin et al., *Pydantic Validation*, version v2.13.0b2, Feb. 2026. [Online]. Available: <https://github.com/pydantic/pydantic>
- [31] Z. Qin et al. “VOLMO: Versatile and Open Large Models for Ophthalmology”. arXiv: 2603.23953 [cs], pre-published.

## 8. AUTHOR CONTRIBUTIONS

Conceptualization: VH, CE, PB; Methodology: VH, CE, PB; Software: VH; Validation: VH; Data Curation: VH; Writing - Original Draft: VH, PB; Writing - Review & Editing: CE; Visualization: VH, PB; Supervision: PB, CE; Funding acquisition: PB

## 9. COMPETING INTERESTS

None to declare.

## 10. ACKNOWLEDGMENTS

We thank Camila Roa, Sarah Müller, Ifeoma Nwabufu, Jan-Niklas Böhm, Fabio Seel, Samuel Ofosu Mensah, Simone Ebert, Rita González Márquez and Julius Gervelmeyer for annotating PubMed-Ophtha-Annotation.

## 11. FUNDING

We thank the Hertie Foundation and the Carl Zeiss Foundation (CZ Nexus: Certification and Foundations of Safe Machine Learning Systems in Healthcare) for funding. PB and CE are members of the Cluster of Excellence 2064 "Machine Learning – New Perspectives for Science" funded by the German Research Foundation (DFG).

## A. FULL DATASET COLUMN DESCRIPTION

**Table 2.** Overview of the fields in the pubmed\_ophtha.parquet file.

Field Name	Type	Content
panel_id	int	Unique ID of the panel
article_id	int	PMC ID of the article (omitting the PMC in the beginning)
image_cluster_id	string	ID of the figure in PMC article
panel_name	string	Name of the panel inferred from the panel identifier
subcaption_text	string	Text of the subcaption
subcaption_segments	list	Indices of the subcaption text in the original caption
panel_image_bytes	binary	PNG image containing the panel
position	string	JSON containing positional information.
is_multi_page_figure	bool	True if the figure stretches across multiple pages
in_text_mention	list	In-text mentions of the figure (from BIOMEDICA dataset)
contains_cfp	bool	True if at least one image in the panel has type CFP
contains_oct	bool	True if at least one image in the panel has type OCT
contains_retinal	bool	True if at least one image in the panel has type Retinal Imaging
contains_other	bool	True if at least one image in the panel has the type Other
contains_marked	bool	True if at least one image in the panel has a mark
image_data	string	JSON containing detected images
identifier_data	string	JSON containing detected panel identifiers
assembly	string	Method of panel assembly
annotation	string	JSON list containing the parts that were humanly annotated (figure, panel, image and caption)
license	string	License under which the paper containing the figure was published
attribution	string	Attribution to the original work
commercial_use	bool	True if the license allows commercial use

**Table 3.** Overview of the fields in the pubmed\_ophtha\_annotation.json file.

Field Name	Type	Content
article_id	int	PMC ID of the article
image_cluster_id	string	ID of the figure in PMC article
figure_locations	list	List containing the pages and positions (in pt) of the figure
caption_locations	list	List containing the pages and positions (in pt) of the captions
panel_data	list	List containing the annotated panels (if available) with their assigned images, labels, and subcaptions
annotation	string	JSON list containing the parts that were humanly annotated (figure, panel, image and caption)
license	string	License under which the paper containing the figure was published
attribution	string	Attribution to the original work

**Table 4.** Overview of the PubMed-Ophtha dataset statistics.

Property	Value
<i>Dataset size</i>	
Articles	15,842
Figures	35,544
Panels	102,023
Number of unique MeSH terms	5,402
<i>Image type distribution</i>	
CFP	24,155 (23.7%)
OCT	43,352 (42.5%)
Retinal Imaging	48,974 (48.0%)
Other	10,705 (10.5%)
<i>Mark status</i>	
Panels with marks	27,534 (27.0%)
<i>Subcaptions</i>	
Mean length (words)	34.1
Median length (words)	28.0
<i>Panel assembly method</i>	
Automatic	68,648 (67.3%)
LLM-refined	32,420 (31.8%)
Manual	371 (0.4%)
PubMed-Ophtha-Annotation	584 (0.6%)

## B. LABELING INTERFACE

The Figures S1 to S3 show the labeling interface in Label Studio in each of the annotation steps.

The screenshot displays the Label Studio interface for annotating a medical document. On the left, a PDF page is shown with red bounding boxes around the figure and caption text. The middle section shows a zoomed-in view of the figure (Cirrus OCT scans) and its corresponding caption and citation text. On the right, a control panel shows the 'Regions' and 'Relations' tabs, with 'By Label' selected. It lists two labels: 'Figure' and 'Caption', each with a 'Box Name' input field. The bottom of the interface has a status bar with labels 'Caption 1', 'Actual Caption 2', 'Figure 3', and 'Actual Figure 4'.

**Figure S1.** Labeling interface during the figure and caption localization. The left side contains a screenshot of the PDF page on which the annotators mark the figure and caption bounding boxes. The right side contains the figure image, caption, and citation from the BIOMEDICA dataset, and an overview of the annotated bounding boxes.

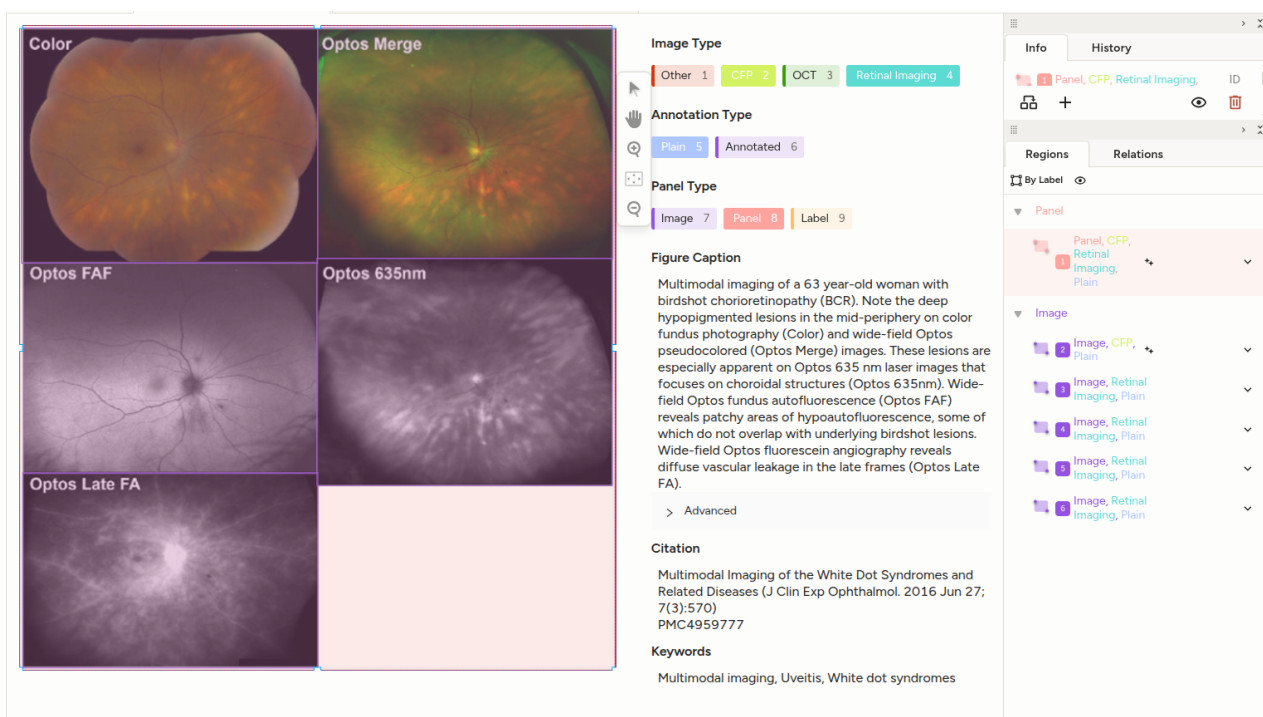


**Figure S2.** Labeling interface during panel and image annotation. The left side contains the figure on which the annotators draw the panel, image, or panel identifier bounding boxes. Right of the figure is the label selection, the figure caption, citation, and keywords. Note that the annotation type and label fields shown in the interface correspond to the mark status and panel identifier in the final dataset, respectively.

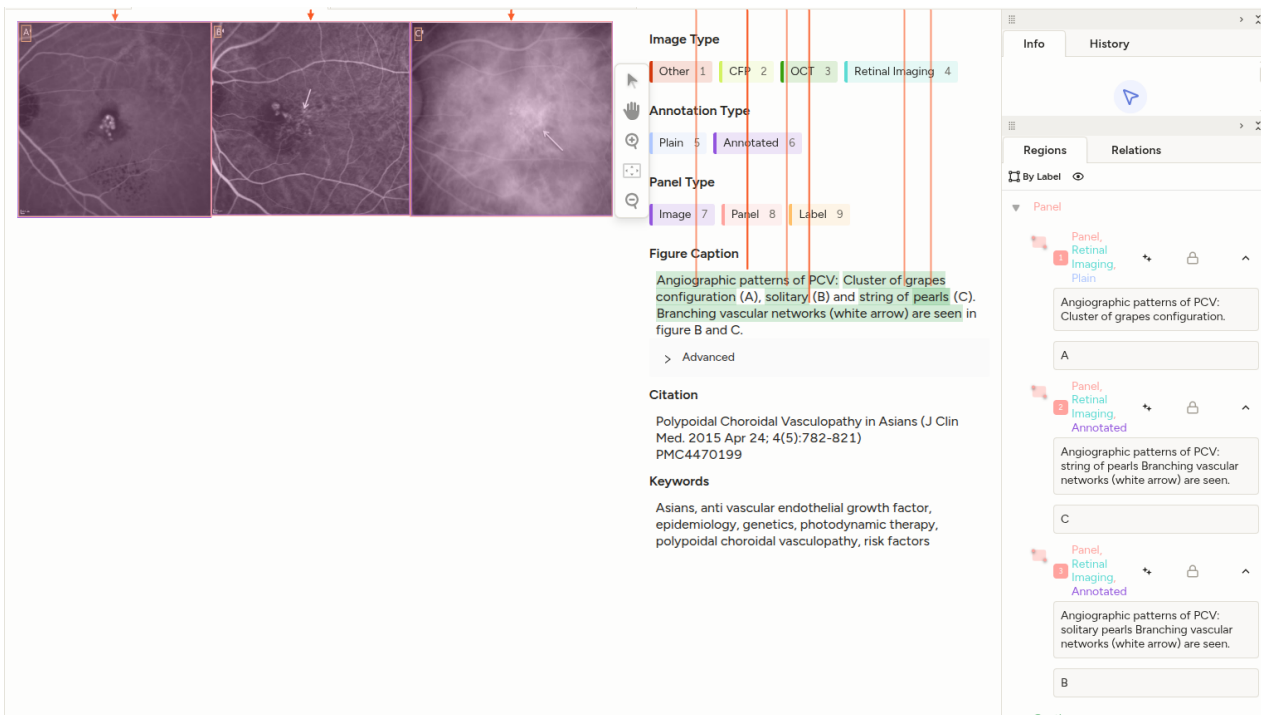


**Figure S3.** Labeling interface during caption annotation. The left side contains the annotated bounding boxes, while the right side contains the label selection, the figure caption, citation, and keywords. The red arrows associate parts of the caption with panels. Each panel bounding box has a free-text field for the subcaption (bottom right).